Earth Planets Space, **61**, 333–343, 2009

Gravity and magnetic constraints on the crustal structure and evolution of the Horeki seamount in the Izu-Ogasawara (Bonin) arc

Toshiya Fujiwara[1], Yukari Kido[2], Yoshihiko Tamura[1], and Osamu Ishizuka[3]

[1]*Institute for Research on Earth Evolution (IFREE), Japan Agency for Marine-Earth Science and Technology (JAMSTEC), Yokosuka 237-0061, Japan*
[2]*Center for Deep Earth Exploration (CDEX), JAMSTEC, Yokohama 236-0001, Japan*
[3]*Geological Survey of Japan, National Institute of Advanced Industrial Science and Technology (AIST), Tsukuba 305-8567, Japan*

(Received July 9, 2007; Revised October 14, 2008; Accepted October 18, 2008; Online published March 3, 2009)

Data on the crustal structure, bulk composition, and eruption ages of an arc seamount were obtained in an investigation aimed at studying the spatial and temporal variations in the magma composition of an intra-oceanic arc. We conducted gravity and magnetic surveys of the Horeki seamount and evaluated the density and magnetization structure using inversion and forward modeling. The seamount is located on the back-arc side of the Izu-Ogasawara arc. This seamount has an elliptical shape, a flat summit, and satellite ridges and cones on its northern and southern flanks. The flanks are consistent with a higher density anomaly, with an estimated mean density corresponding to dense basaltic rocks. A low-density anomaly is distributed in the seamount top, indicating that the top likely consists of porous basalts or differentiated rocks. The prominent circular low Bouguer gravity anomaly, which appeared in the northern part of the flat-topped summit, indicates that a light-density material fills the summit. The main body of seamount is normally magnetized. Combined with the age of the rocks, the volcanism constructing the main body may be most robust in the Gauss chron. The deeper part of seamount may consist of intrusive rocks, with induced magnetization over remanence. The eastern part of the northern ridges is reversely magnetized, while the western part is normally magnetized. These features and the ages of the sampled rocks suggest that these ridges were constructed in the Matuyama and Brunhes chrons, respectively. The southern part of the seamount flanks shows weak normal magnetization, probably caused by the small cones with different polarities of remanent magnetization.
Key words: Horeki seamount, Izu-Ogasawara (Bonin) arc, gravity anomaly, magnetic anomaly, crustal structure.

1. Introduction

The Izu-Ogasawara arc is an active, approximately 1200-km-long intra-oceanic arc associated with Pacific-Philippine Sea plate convergence in the western Pacific (Fig. 1). The Izu-Ogasawara arc is one of the best areas to study intra-oceanic arc evolution and continental crust formation because it is a juvenile arc, its tectonic evolution is better known than that of many others, and it is the best surveyed intra-oceanic arc (e.g., Tatsumi, 2005).

A research group in IFREE JAMSTEC, in collaboration with other Japanese and overseas institutions, has recently conducted an extensive geological and geophysical survey aimed investigating intra-oceanic arc evolution and continental crust formation. We have surveyed several seamounts on the volcanic front and the back-arc ridges and have determined the active periods and geochemical characters of these volcanoes (e.g., Ishizuka *et al*., 2002, 2003a, b, 2006, 2007). A comparison of these volcanoes is essential to any investigation of spatial (across- and along-arc) and temporal variations in the magma composition of this intra-oceanic arc. We have investigated the frontal volcanoes—Sumisu (Tamura *et al*., 2005; Shukuno *et al*., 2006; Tani *et al*., 2008), Torishima island (Tamura *et al*., 2007), and the back-arc Horeki seamount (Tamura *et al*., 2006; Tamura *et al*., in preparation) (Fig. 1). These three volcanoes are similar in terms of size and isolated edifices. Consequently, they can collectively provide two-dimensional information relating to arc magma genesis in an environment that is only contaminated by complex, pre-volcanic histories to a very small degree.

The geophysical surveys consisted of whole crustal-scale seismic experiments, resulting in the development of several profiles of the crustal structure along and across the arc (e.g., Park *et al*., 2002; Takahashi *et al*., 2005; Tsuru *et al*., 2005; Kaiho *et al*., 2006; Miura *et al*., 2006; Nishizawa *et al*., 2006; Kodaira *et al*., 2007a, b). Detailed surveys of multibeam bathymetry, gravity, magnetics, seismics, and heatflow around rock dredge sites or submersible/ROV diving survey sites were also carried out (e.g., Kido, 2005). Those surveys have provided valuable data for assessing magma genesis, crustal evolution, and their variation along and across the whole arc.

Here, we present gravity and magnetic data on the Horeki seamount that was collected in a 2004 survey aboard the R/V *Kairei* (KR04-04 cruise). The geological observations and rock samplings were made within confined areas. To validate the observations, we also carried out a gravity and magnetic study to provide constraints on the crustal struc-

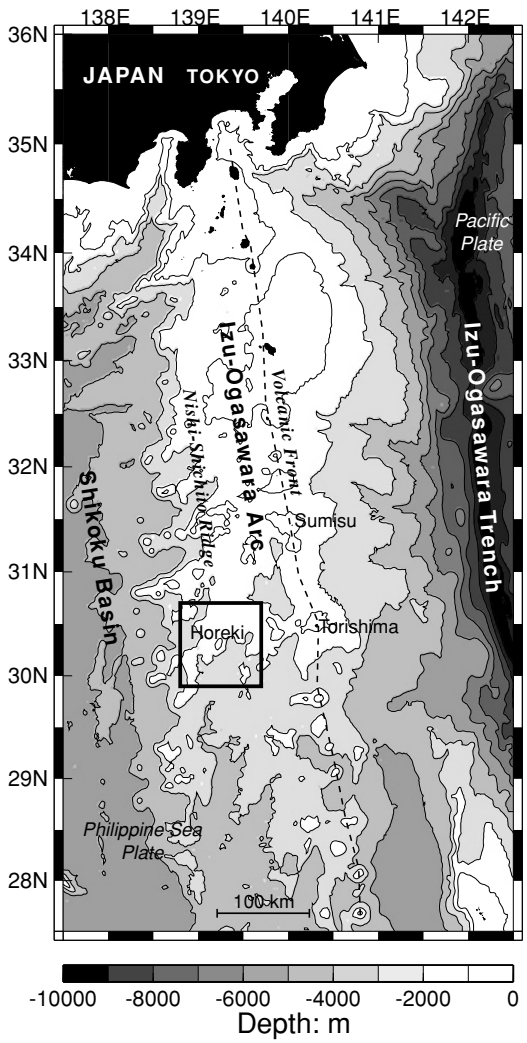

Fig. 1. Bathymetry of the northern Izu-Ogasawara arc showing the location of the Horeki seamount. The black square shows the survey area.

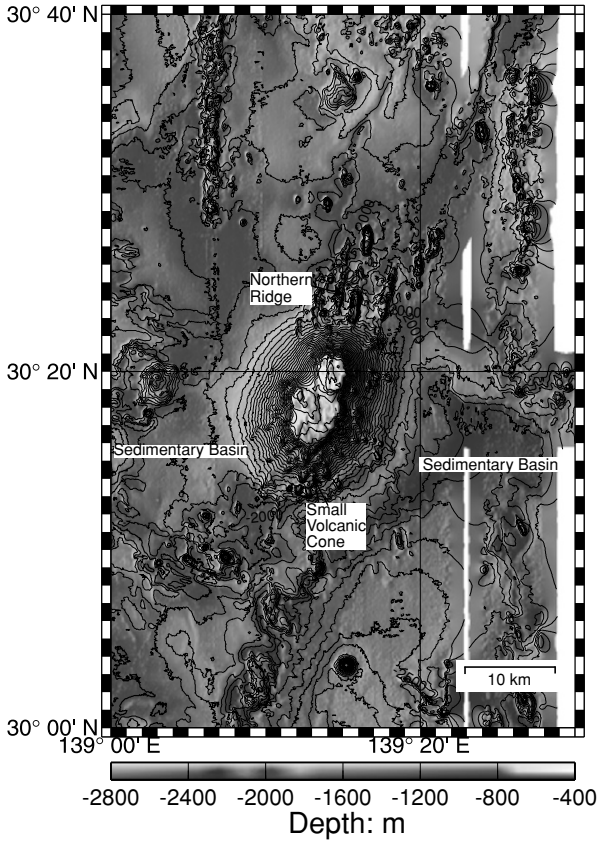

Fig. 2. Detailed bathymetry of the Horeki seamount. Contour interval is 50 m. Thick contour lines are plotted in the 500-m interval.

ture, bulk composition of the seamount, eruption ages, and a robust estimate of volcanic output with times.

2. Geological Setting

The Horeki seamount is a back-arc seamount located approximately 100 km W-SW of Torishima island in the northern Izu-Ogasawara arc (Fig. 1). At a depth of 1800–2000 m, the main body of the Horeki seamount has an elliptical base of approximately 25 km long and approximately 15 km wide (Fig. 2). The seamount elongates in a NNE-SSW direction. The flat summit at a depth of 400–700 m is approximately 10 km long and approximately 5 km wide. The relative height of the seamount is approximately 1500 m. The seamount has many satellite cones or knolls, especially on its northern and southern flanks. The northern knolls form parallel ridges trending NNE-SSW, and the southern cones, with diameters of approximately 1 km, are distributed radially from the center of the main body.

Rock samples were collected by dredges and the ROV *Hyper-Dolphin* (white circles and squares; Fig. 3). The sampled rocks show that the main components of the Horeki seamount are basaltic and andesitic rocks. Basalts from the main body are medium-K and demonstrate arc-like features. In contrast, basalts from the northern ridges and the southern lateral cones are low-K and show MORB-like (BABB) features (Tamura *et al.*, 2006).

An ^{40}Ar-^{39}Ar study of the sampled rocks indicated that the ages of the main body of the seamount are approx. 3.6–3.0 Ma (3.62±0.06 to approx. 3.05±0.02 Ma; these plateau ages were determined with an accuracy of <0.1 m.y.) (Fig. 3). Other ridges and cones are younger: approx. 3.0–2.0 Ma or 0.5 Ma (3.02±0.18 to approx. 2.07±0.10 Ma; 0.48±0.03 Ma) (O. Ishizuka, unpublished data, 2006).

A multi-channel seismic (MCS) line of the R/V *Kairei* KR02-05 cruise crosses over the northern portion of the seamount (Park *et al.*, 2002) (white line, Fig. 3). A single-channel seismics is also obtained on the same line. The deep internal structure of the seamount is not evident because of the absence of clear reflections and multiple reflections (Fig. 4). The MCS seismic reflection shows sedimentary basins to the west and east of the seamount. Acoustically transparent upper layers are probably hemipelagic sediments, and the lower layers are volcanic debris. The thickness of these sedimentary basins is estimated to be 0.6–0.8 km and 0.8–1.0 km, respectively. In the northern flat-topped summit (arrows, Fig. 4), seismic reflections are identified at approximately 0.15 s (two-way travel time: TWT) beneath the summit. The reflections may be due to an acoustic impedance (density contrast) boundary beneath the summit.

A refraction seismic survey with ocean bottom seismometers (OBSs) on the same line as the MCS line de-

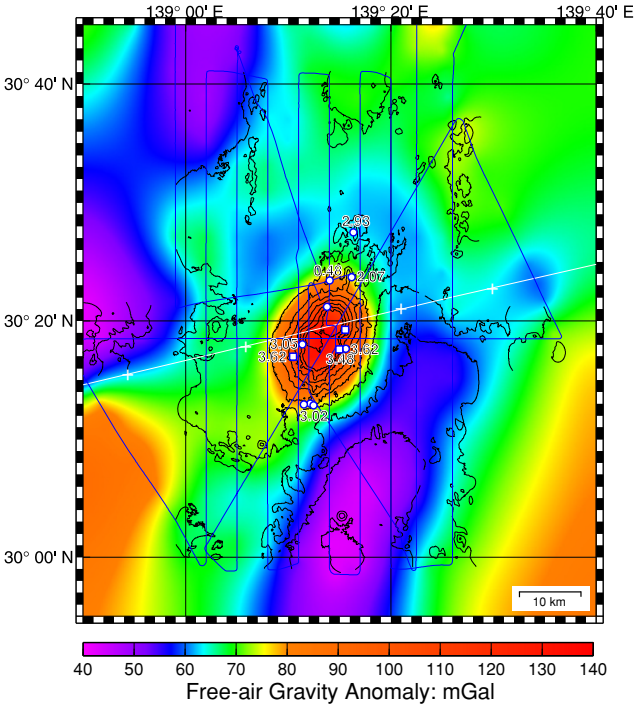

Fig. 3. Colored image of free-air gravity anomaly of the Horeki seamount. Black contour lines delineate bathymetry with 200-m intervals. Blue and white lines show the ship tracks of KR04-04 and a multi-channel seismic (MCS) line of KR02-05, respectively. White crosses show the locations of the deployed ocean bottom seismometers (OBSs). White circles and squares show the locations of rock samples obtained during KR04-04 and NT04-10 cruises. The circles and squares indicate the locations where basalts and andesites were mainly obtained, respectively. Attached numbers indicate their rock ages in Ma (O. Ishizuka, unpublished data, 2006).

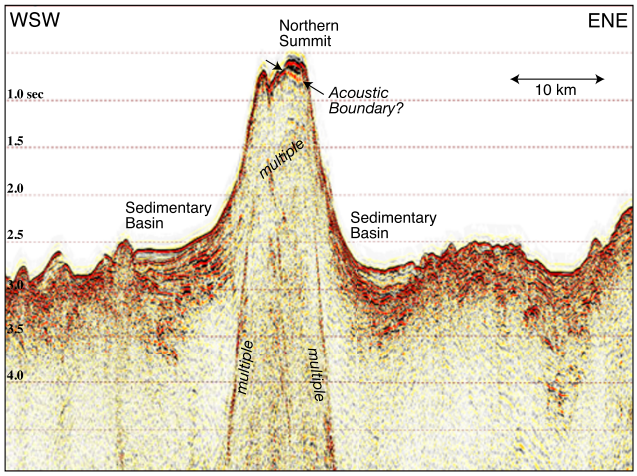

Fig. 4. Seismic profile of KR02-05 (see Fig. 3 for the location). The vertical axis indicates two-way travel time (s).

picts the velocity structure of the typical island arc crust with a thickness of approximately 20 km in this portion (Nishizawa *et al.*, 2006). The island arc consists of an upper crust approximately 5 km thick with a P-wave velocity (V_p) < 6.0 km/s, a middle crust approximately 5 km thick with a velocity of 6.0–6.3 km/s, and a lower crust approximately 10 km thick with a velocity of 6.8–7.2 km/s. The interval of the OBSs around the Horeki seamount was greater than 25 km, and no OBS was deployed on the seamount (crosses, Fig. 3). Thus, the OBS deployment provides rather sparse data to reveal the local variation of the velocity structure of the Horeki seamount.

3. Data Collection

The main survey tracks are aligned in the north-south direction with a spacing of 3 miles (approx. 4.8 km) (blue lines, Fig. 3). Swath bathymetric data were obtained using a *SeaBeam 2112* multi-narrow beam echo sounder system. The survey covered an area of approximately 80 km in the north-south direction and approximately 50 km in the east-west direction centered at the Horeki seamount.

Onboard gravity measurements were conducted using a *Bodenseewerke KSS-31* marine gravity meter. Gravity data were collected throughout the cruise. The speed of the ship was about 10 knots. The data were recorded every 1 min (approx. 300 m). The free-air gravity anomaly was calculated by subtracting the theoretical gravity formula of the Geodetic Reference System 1967 (International Association of Geodesy (IAG), 1967) from the collected data (Fig. 3). Crossover errors (COEs) at 81 track crossing points in this cruise yielded an RMS standard deviation of 2.2 mGal. Details of the gravity measurements are given in Fujiwara *et al.* (2006).

Geomagnetic total force data were obtained using a surface-towed proton precession magnetometer *PROTO10* (Kawasaki Geol. Eng. Co.). The sensor was towed 300 m behind the ship, and the data were collected every 20 s (approx. 100 m). The geomagnetic total force anomaly was calculated by subtracting the International Geomagnetic

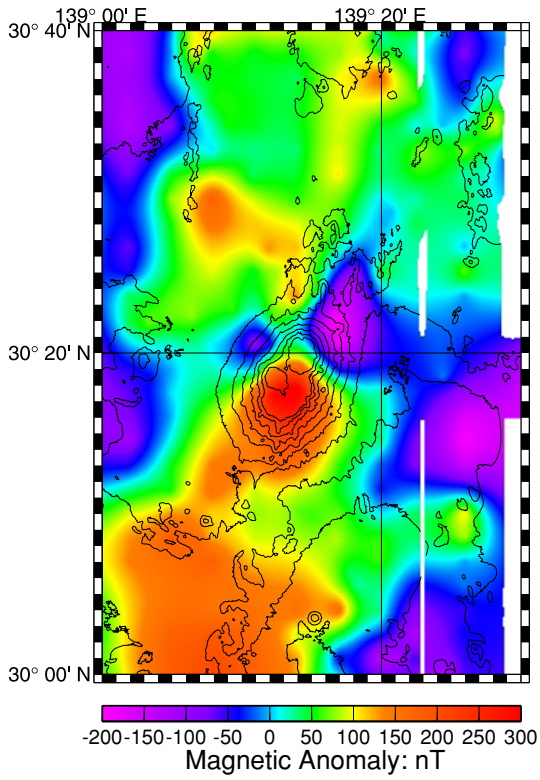

Fig. 5. Colored image of magnetic anomaly of the Horeki seamount. Black contour lines delineate bathymetry with 200-m intervals.

Reference Field (IGRF) 9th generation (International Association of Geomagnetism and Aeronomy (IAGA), 2003) (Fig. 5). The COEs at 46 track crossing points in this cruise yielded an RMS standard deviation of 13.9 nT. Referring to the K_p indices, the survey dates (April 18–20, 2004) are classified as magnetic quiet days. Corrections in diurnal variation were conducted using observed geomagnetic data at the Hachijo Hydrographic Observatory located in approximately 300 km north of the survey area. After the correction, the standard deviation was reduced to 5.2 nT.

4. Gravity and Magnetic Anomalies

4.1 Gravity

To examine sub-seafloor density variations, we first calculated the Bouguer gravity anomaly from free-air gravity by subtracting the predicted gravity effects of seafloor topography using the method of Kuo and Forsyth (1988), Prince and Forsyth (1988), and Lin *et al.* (1990). The observed free-air gravity anomaly data were merged with the gravity anomaly data derived from satellite altimetry (Sandwell and Smith, 1997) to extend coverage to areas where no shipboard gravity data were available. For a similar reason, bathymetric data of JTOPO30 were merged with the observed swath bathymetry. Note that the extended area was not included for interpretations. The topography was gridded at approximately 180 m for the Bouguer gravity calculation. To avoid artificial edge effects, we mirrored the grid both east-west and north-south. The assumed density for the gravity calculation was estimated using a G-H (gravity-water depth) correlation. The result shows that the calculated Bouguer gravity anomaly with the assumed density of 2510 kg/m^3 has the lowest correlation with variations in water depth (topography) in the area around the seamount (30 × 30 km).

The long-wavelength Bouguer gravity anomaly shown in Fig. 6(a) reflects the variation in the crustal thickness of the Izu-Ogasawara arc (e.g., Ueda, 1996; Geological Survey of Japan, 2000; Fujiwara, 2004). The gravity anomaly value gradually increases from north to south in accordance with a decrease in the crustal thickness. Recent seismic refraction surveys confirm this variation in thickness (Kodaira *et al.*, 2007a, b). The long-wavelength variation in the gravity anomaly is removed by a linear trend approximation. The residual gravity anomaly is supposed to be caused by a subsurface density structure of the Horeki seamount (Fig. 6(b)).

The flanks of the seamount are associated with a higher than average gravity anomaly, up to approx. 5–10 mGal in amplitude (Fig. 6(b)). In contrast, low anomaly extends parallel to the long axis (NNE-SSW) in the top part of the seamount. A prominent feature is a circular low anomaly that is up to 15 mGal in amplitude and approximately 5 km in diameter, which appears in the northern part of the flat-topped summit. A slightly circular low anomaly is also found in the central part of the flat-topped summit. To the west and east of the seamount, the sedimentary basins are accompanied by a low anomaly with an amplitude of about −5 mGal.

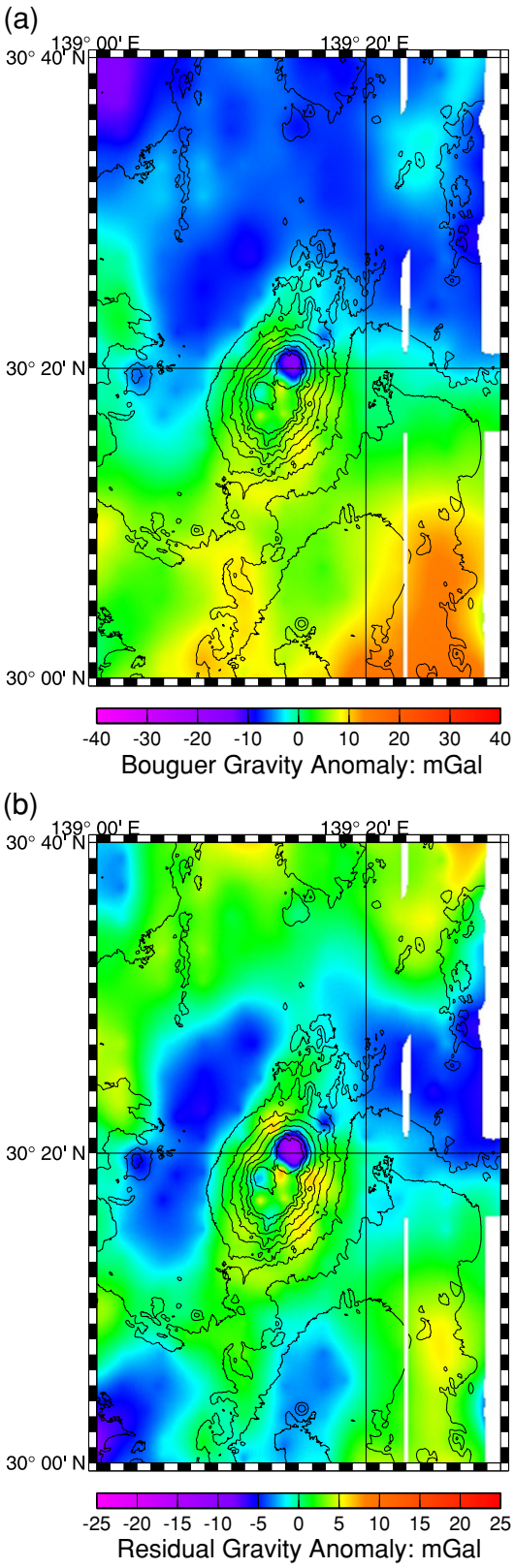

Fig. 6. Colored images of Bouguer gravity anomaly (a) and residual Bouguer gravity anomaly (b) of the Horeki seamount. Black lines show topographic contours that outline the seamount.

4.2 Magnetics

A long-wavelength positive anomaly extends in the north-south direction (Fig. 5). The long-wavelength anomaly may be due to deeper sources extending along the Nishi-Shichito ridge (the western fringe of the Izu-Ogasawara arc: see Fig. 1 for the location) (Yamazaki and Yuasa, 1998). Short-wavelength anomalies probably

caused by the Horeki seamount are superimposed on the long-wavelength anomaly. The long-wavelength magnetic anomaly is removed by a bandpass filter with cosine taper for wavelengths between 40–80 km. The positive peak of the short-wavelength anomaly is centered on the southern part of seamount and the western part of the northern ridges. The negative trough is located to the NE of the seamount and on the NW flank. The peak-to-trough amplitude of the anomaly is approximately 500 nT.

5. Data Analyses

5.1 Density/magnetization modeling

We performed bulk density/magnetization modeling that mainly reflects the general distribution of density/magnetization near the seafloor, since no strong geological or geophysical constraint on depth distribution of density/magnetization beneath the Horeki seamount is available. Our analysis of the density/magnetization structure was accomplished using inversion of the gravity/magnetic anomalies. A crustal model consists of a set of prism-shaped bodies as shown in Fig. 7. The calculated gravity/magnetic anomaly can be written in matrix form as

$$\mathbf{F} = \mathbf{G} \bullet \mathbf{m} \tag{1}$$

where the bold dot denotes matrix multiplication, **F** and **m** are the calculated gravity/magnetic anomalies and density/magnetization written as column vectors, respectively, and **G** is a matrix concerned with the geometric relation between the observation points and prisms. The elements in **G** can be calculated using a formulation of Bhattacharyya (1964) and Blakely (1996).

In the case shown in Fig. 7, Eq. (1) becomes a set of linear algebraic equations:

$$\mathbf{F}_i = \mathbf{G}_{ij} \bullet \mathbf{m}_j \ (i = 1, 2, \ldots, N;\ j = 1, 2, \ldots, M) \tag{2}$$

where N is the total number of observations, and M is the total number of prism-shaped bodies. The unknown $\mathbf{m}_j$ can be inverted by solving the least squares method under the condition of $N > M$. A technique of singular value decomposition is applied to solve Eq. (2) (Press *et al.*, 1992).

Observed gravity/magnetic data were gridded at 1.0-km spacing for the inversion. The observation points are distributed within the 30-km square ($N = 961$ (31×31)) (Fig. 7). A unit prism is 0.5×0.5 km in horizontal extent. Each prism has a uniform density or magnetization. The resolution of analysis depends on the water depth and the interval of the survey ship tracks, as shown in Fig. 8. As a first step, in the inversion, a prism model of 2.5×2.5 km in the horizontal plane was adopted to reduce the number of models (M) and to suppress oscillatory solutions at deeper depths. The prism model comprised a set of 0.5-km-grid prisms; therefore, finer 0.5 km-grid topography was taken into account and preserved (Fig. 7). These prisms are distributed within the 47.5-km square, including surrounding areas ($M = 361$ (19×19)).

Successively, 1.5×1.5-km prisms were reorganized within the 25.5-km square ($M = 289$ (17×17)) to improve the resolution in the area of shallower depth around the Horeki seamount (Fig. 7). The prism model was organized by modifying partitions of the set of prisms. Note that the configuration of the basic 0.5-km-size prisms was not changed. The $\mathbf{m}_j$ was corrected by $\Delta\mathbf{m}_j$, which was solved from the following equation.

$$\mathbf{d}_i = \mathbf{G}_{ij} \bullet \Delta\mathbf{m}_j \ (i = 1, 2, \ldots, N;\ j = 1, 2, \ldots, M) \tag{3}$$

where $\mathbf{d}_i$ is the residual between observed gravity/magnetic anomalies and calculated anomalies using the previous model, and $\Delta\mathbf{m}_j$ is the correction of density/magnetization. The $\mathbf{G}_{ij}$ represents the gravity/magnetic anomaly at point i due to prism j with unit density/magnetization.

In addition, boundary lines for the prism partition were shifted to modify the set of prisms in order to minimize the effects of locations of the partition (Fig. 7). Therefore, the final solution was achieved by an iterative improvement process. The area of shallow water depth (i.e., the Horeki seamount) was solved using 0.5-km size prisms in the final analyses. High-cut filtering by the distance-weighted mean was operated to suppress high-frequency oscillation in an ill-conditioned case. Note that the calculation areas were broader than areas shown in resultant figures in later sections to avoid side effects from actual sources surrounding the areas.

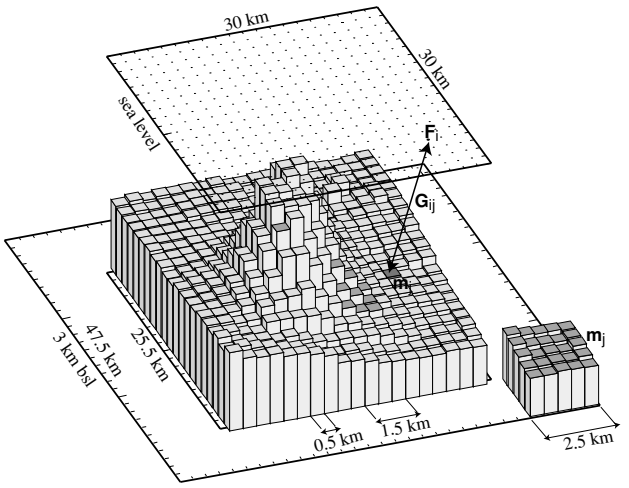

Fig. 7. Schematic illustration of the model used in the inversion analysis. Observation points for the inversion are distributed within the 30-km square at 1.0-km spacing. Crust is modeled as a set of prism-shaped bodies. A unit prism is 0.5×0.5-km in the horizontal extent. Their upper faces follow the seafloor. The bottom of prisms is set to be 3 km below sea level (bsl). Note that prisms also extend all around the area of the 47.5-km square. In the inversion, a prism model of 2.5×2.5 km in the horizontal plane is adopted within the whole area. In the 25.5-km square inner area, 1.5×1.5-km prisms are organized. The area of shallow water depth (i.e., the Horeki seamount) is solved with 0.5-km size prisms.

5.2 Parameters for gravity/magnetic inversions

As for parameters of the gravity inversion, the bottom of the model layer was set to be at a constant depth of 3 km below sea level (Fig. 7). The bottom depth is determined by the thickness of the layers in the sedimentary basins (approx. 1 km) at the base water depth (approx. 2 km). Therefore, a large density change is expected down to this depth. The layer deeper than this depth is rather homogeneous based on seismic studies (Park *et al.*, 2002; Nishizawa *et al.*, 2006). The assumption made on the layer thickness may be

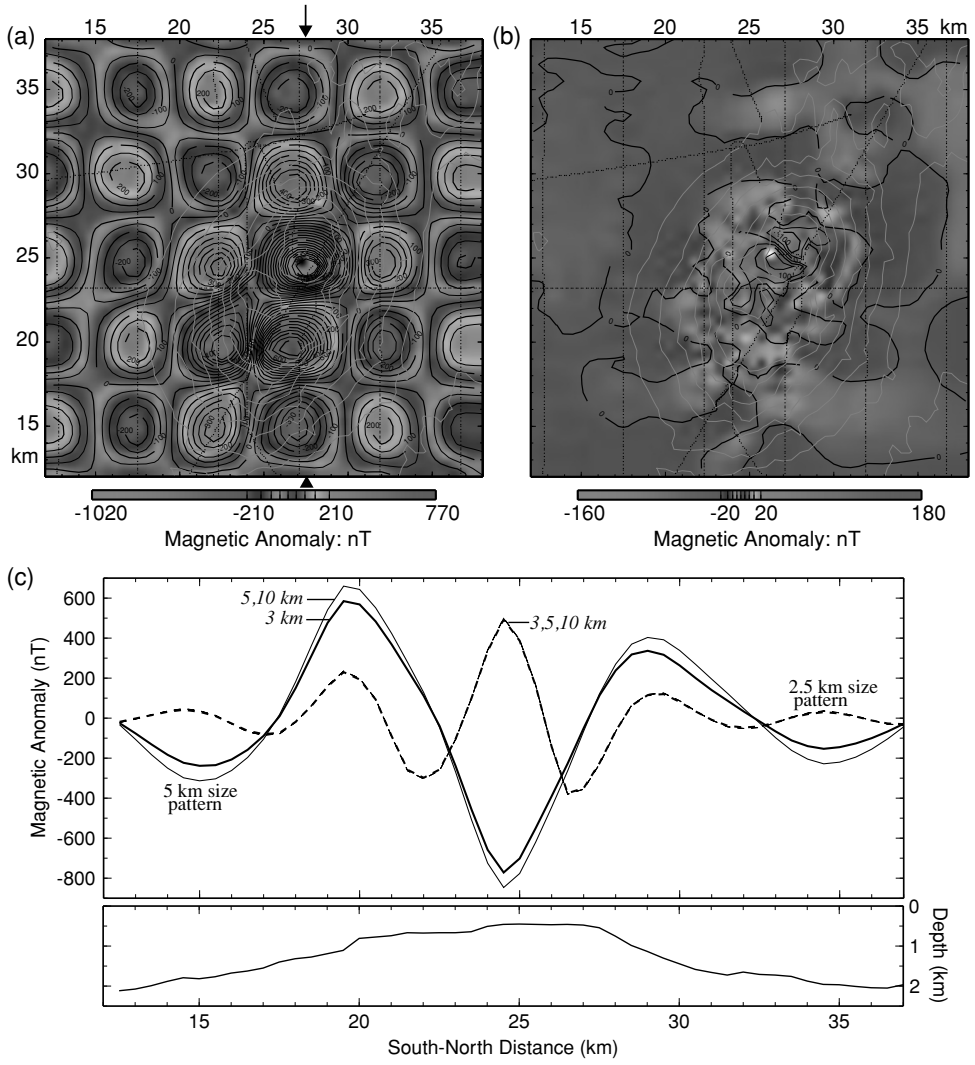

Fig. 8. Magnetic anomaly due to prism-shaped bodies of which the upper faces follow the Horeki bathymetry (red contours). The anomaly was calculated at actual observation points along the ship tracks (black dots). Contour interval of the magnetic anomalies is 50 nT. Magnetization has a 5-km-size checkerboard-like (-2 and $+2$ A/m) pattern (a) and the anomaly reflects well the magnetization structure. Arrows in (a) point to the longitude track at 27.5 km shown in (c). In terms of the 1-km size checkerboard pattern (b), the checkerboard pattern does not appear in the magnetic anomaly in the area of deep water depth. Comparison of magnetic anomaly profiles along the longitude track at 27.5 km is shown in (c). The anomalies are due to checkerboard-like magnetization with different bottom depths (3, 5, and 10 km bsl). In the case of a 2.5-km size pattern (broken lines), a significant difference is not distinguished among the different depth models. In the case of the 5-km size pattern (solid lines), as shown in (a), the 5-km and 10-km depth models show almost no difference. The amplitude of magnetic anomaly with the 5-km depth model is approx. 80 nT larger than that of 3 km. That is only approximately 5% of the peak-to-trough amplitude of the magnetic anomaly despite the fact that the magnetized layer increases are twofold thicker. The lower panel shows the topography of the Horeki seamount along the track.

inappropriate in some places. The choice of another layer thickness would result in different density magnitudes but would not significantly affect the variation of the density distribution.

In terms of parameters in the magnetic inversion, as the seamount was formed recently—between approximately 3 Ma and approximately 0.5 Ma according to our analysis of the age of the rock—no significant drift and rotation of the seamount, associated with the evolution of the northern Izu-Ogasawara arc are expected (Koyama *et al.*, 1992). Thus, the direction of magnetization in the source layer was reasonably assumed to be oriented parallel to a geocentric dipole field at the present latitude (declination 0° and inclination 49°). The ambient geomagnetic field was set to a declination of $-5°$ and inclination of 42° with reference to the International Geomagnetic Reference Field (IGRF). The bottom depth for the magnetization model corresponds to 3 km below sea level. In our case, since the magnetic anomaly is obtained at the sea surface above a 2-km water depth, and the effect of sources at 2 km below the seafloor is much smaller than that of surface sources. Therefore, even if we selected a thicker vertical size for the assumed sources in the analysis, the result would differ only slightly (Fig. 8(c)).

6. Results and Discussion

6.1 Density structure

The calculated density structure is shown in Fig. 9. The root mean square (RMS) of the residual between the calculated and observed gravity anomalies is 3.1 mGal. The colors indicate a density difference from the assumed density of 2510 kg/m^3 for the calculation of Bouguer grav-

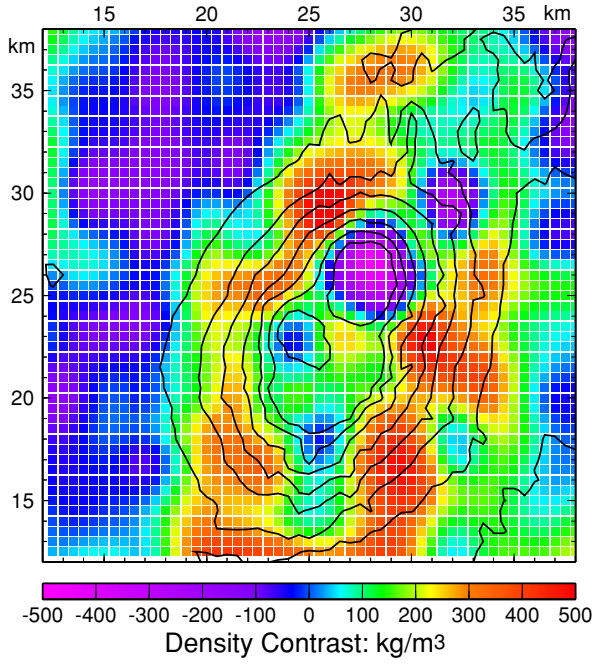

Fig. 9. Colored image of density structure of the Horeki seamount. The colors indicate a density difference from the assumed density of 2510 kg/m^3. The colored tiles show the architecture of the prism models with 0.5 × 0.5 km in the horizontal plane. Solid lines show 200-m bathymetric contours and outline the Horeki seamount.

ity anomaly. The flanks of the seamount are consistent with a higher density anomaly, with a range from +300 to +400 kg/m^3. The resultant density corresponds to dense basaltic rocks of approx. 2800–2900 kg/m^3. In fact, the mean density of the basaltic rock samples is 2.77 g/cm^3 (2770 kg/m^3).

Compared with the seamount flanks, a lower density anomaly is distributed in the top part of the seamount, extending in the NNE-SSW direction, parallel to the long axis of the seamount. The resultant density is equal to or slightly higher (+100 kg/m^3) than the assumed density of 2510 kg/m^3. The degree of density would be consistent with that of common andesitic-basaltic rock, 2700–2800 kg/m^3, taking into consideration a porosity of approximately ±10% (e.g., Shipboard Scientific Party, Site 1256, 2003).

It is possible that volcanic lavas erupting in shallow water depths tend to have higher porosity (i.e., lower density) than those erupting in greater depths because the pressure from the weight of the water against the gas pressure in the magma is smaller in the shallow depths. The degree of porosity might be the origin of the density structure, which is a high-density anomaly of the flanks of the seamount in deeper depths and a low-density anomaly in the top part of the seamount.

An alternative possibility is that the top part of the seamount mainly consists of more differentiated rocks. Although the sampled rocks are basalts and andesites, there are too few rock sampling sites to draw any conclusion on the main component.

The prominent circular low anomaly, which appeared in the northern part of flat-topped summit, requires light-density material filling the summit. The result indicates that the density is less than 2100 kg/m^3. Because the observed low-gravity anomaly is rather locally distributed and the short-wavelength is dominant, as shown in Fig. 6(b), lighter densities, such as those of approx. 1000–2000 kg/m^3, and thinner layers, such as those of approx. 0.3–1.0 km, may be required as the anomaly sources for the circular low anomaly (Fig. 10). The actual bottom of the low-density layer is not determined. The seismic reflection in the MCS profile at 0.15-s TWT beneath the flat-topped summit, discussed in Section 2 (Fig. 4), is too shallow to be considered as the interface of the basement. Because velocity in the low-density layer is likely to be $V_p \sim$ 1.8–2.0 km/s (Ludwig *et al.*, 1970), the travel time corresponds to approx. 135–150 m in depth. A forward model with the layer thickness of 0.15 km, where the seismic reflection is observed, produces quite a small amplitude of low anomaly, even in the presence of a low density (1000 kg/m^3) almost equal to water density (Fig. 10).

The circular shape of the density anomaly on the flat-topped seamount suggests that the seamount is a guyot and that the summit protruded above the sea level in the past. During a certain period, the top of the seamount was planed by waves, and light material deposition, such as coral reef formation, piling up of phosphate rocks, and/or other processes, occurred.

A crater is also a probable cause of the circular low anomaly. Sub-aqueous volcanoes can produce volcanic ash if they reach shallow water depths, and the ash and scoria then fill the crater floor. A caldera may be completely filled by such volcanic ash and/or scoria as the cause of the circular low anomaly. However, this interpretation contradicts a typical feature of gravity anomaly of basaltic volcanoes. Calderas and ridges of basaltic volcanoes, which are the possible direction of dyke fissures, are commonly associated with high-gravity anomalies in the northern Izu-Ogasawara arc (e.g., Murakami and Ishihara, 1985), because dense lava flows fill the caldera floors and dyke swarms intrude in the fissures.

Low-density anomalies of −100 kg/m^3 are consistent with the sedimentary basins. The sedimentary basins deduced from the MCS result are landslide deposits made of volcanic lava and hemipelagic sediments (Park *et al.*, 2002).

6.2 Magnetization structure

Calculated crustal magnetization is shown in Fig. 11. The RMS of the residual between the calculated and observed magnetic anomalies is 3.8 nT. The main body of the seamount is normally magnetized. Its magnetization intensity is calculated to be approx. 1.5 A/m. The intensity seems to be notably small considering extrusive volcanic lavas are the source of the magnetic anomaly. For example, the natural remnant magnetization (NRM) of some basaltic lava samples that were collected at the northernmost sampling location shown in Fig. 11 was 11.2 A/m on average.

If the seamount body mainly consists of extrusive lavas, the calculated magnetization could be an average of each magnetized layer to the depth or the horizontal plane. Each layer has an NRM and an induced magnetization (IM), including viscous remanent magnetization (normal magnetization). Because the seamount consists of volcanic lavas

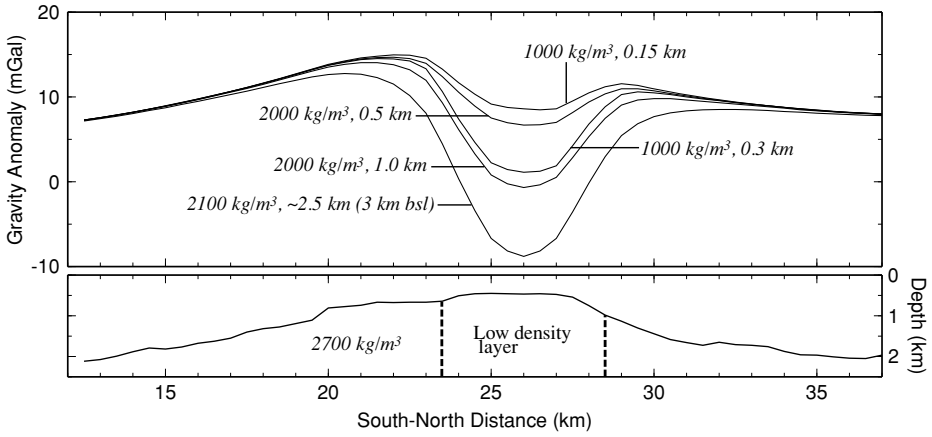

Fig. 10. Comparison of gravity anomaly profiles along the longitude track. The location of the track is presented in Fig. 8(a). The anomalies calculated by forward gravity modeling are due to cylindrical layers with different densities and thickness to examine the observed circular low anomaly. The cylindrical layers extend 5 km in diameter centered at 26 km in the figure. The density in the circum-Horeki seamount is set to be 2700 kg/m^3. A parameter combination of a density of 2100 kg/m^3 and a thickness of approximately 2.5 km (3 km bsl) is derived from the inversion result. In this case, the resultant low-gravity anomaly is widespread. The cause is that the anomaly source is distributed to the deeper depth. Adoption of anomaly sources with lighter densities, such as 1000–2000 kg/m^3, and thinner layers, such as 0.3–1.0 km, accomplishes the short-wavelength, low-gravity anomaly with an amplitude as large as 15 mGal of dent in the anomaly. A model with the layer thickness of 0.15 km produces quite a small amplitude of low anomaly even in the low density (1000 kg/m^3) region. The lower panel shows the topography of the Horeki seamount along the track and location of the low-density layer.

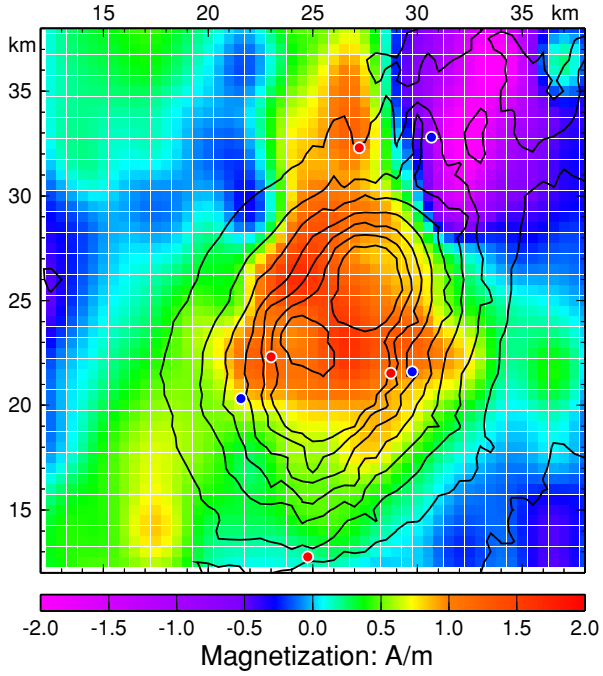

Fig. 11. Colored image of crustal magnetization of the Horeki seamount. The colored tiles show the architecture of the prism models with 0.5×0.5 km in the horizontal direction. Red and blue circles denote rock sampling locations. The ages of the rocks in the normal chron are shown by red circles and reverse ones in blue circles, respectively. Solid lines show 200-m bathymetric contours and outline the Horeki seamount.

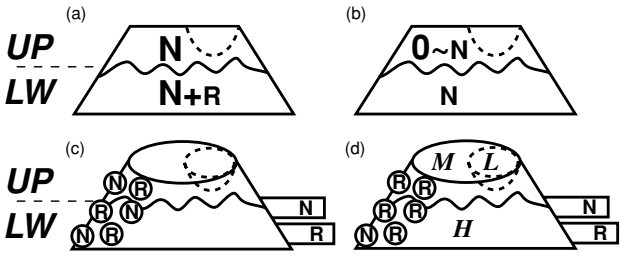

Fig. 12. Comparison between magnetization models of the Horeki seamount. Trapezoids show seamounts looking from the SE. Solid lines in the seamounts show boundaries between UP and LW. UP is an upper or surface layer, and LW is a lower or inner layer of the seamount. Broken lines in the seamounts delineate low-density layers on the summits. Note that these boundary lines are schematic and not real. N, 0, and R indicate normal, non/weak, and reversed magnetization, respectively. Models for the main body (a) and (b) could explain the calculated magnetization intensity. (c) and (d) are schematic models showing two possible origins of the magnetization in the northern ridges and the southern part of seamount flanks. Rectangles in the right side show the northern ridges, the rectangles in the top are the western part of the ridge and thosein the bottom are the eastern part. Circles in the left side represent small cones. L, M, H in (d) indicate high density, respectively.

erupted in various ages, the NRM obtained in a magnetic polarity chron could cancel the effect of one in another polarity chron. As the result, the lower magnitude in magnetization is considered to be produced in the analytic model that we adopted, assuming uniform magnetization.

Eruption ages of the Horeki seamount range over four major magnetic chrons starting from Gilbert (reverse polarity), Gauss (normal), and Matuyama (reverse) to Brunhes (normal) (Cande and Kent, 1995). The main body of the seamount is probably constructed in Gilbert (5.23–3.58 Ma) and Gauss (3.58–2.58 Ma), according to our analysis of the ages of the rocks (O. Ishizuka, unpublished data, 2006) (Figs. 3, 11). The resultant (surviving) normal magnetization indicates that the volcanic rocks magnetized normally are more abundant and that the volcanism constructing the main body may be more robust in Gauss normal chron (Fig. 12(a)).

Even if the seamount body mainly consists of extrusive lavas and the lavas magnetized normally are much robust, the top part of the seamount may be made of more differentiated rocks, as is suggested by the density struc-

ture. These rocks have lower magnetization intensity than basaltic rocks. In this case, the derived magnetization intensity is consistent with the differentiated rocks (Fig. 12(b)).

Otherwise, as the high-density portions (>2800 kg/m^3) are estimated in the flank of the seamount, the deeper and inner part of the seamount may consist of intrusive rocks. The intrusive rocks having IM contribute to the normal magnetization. The NRM carried by extrusive lavas does not affect the bulk magnetization intensity due to mixing of normal and reversed magnetization. An alternative is that the more differentiated rocks are the main constituent of the upper part of the seamount, as mentioned above (Fig. 12(b)).

The magnetization structure is not distinct in the northern part of the flat-topped summit, where the prominent circular gravity low appeared. This fact suggests that there is no sharp contrast between the area of low circular gravity and the other summit area in terms of magnetization. Based on the results of both the gravity and magnetic analyses, the crustal structure and the material existing in the summit area are constrained. The summit was filled with volcanic porous deposits, such as scoriae, which could have some degree of NRM and/or induced magnetization to contribute to the normal magnetization in the area (Fig. 12(a)). It would be implausible that the layers of the circular area and the surrounding area have a similar magnetization intensity by coincidence, because materials existing in these layers have quite different densities. Otherwise, if a very low density and a very low magnetization material, such as coral reefs or phosphate rocks, forms the circular layer, the surrounding top part of the summit should have very low magnetization in agreement with the circular layer (Fig. 12(b)).

Ueda (2007) studied a number of seamounts in the Izu-Ogasawara arc and the Kyushu-Palau ridge. The Kyushu-Palau ridge is a conjugate paleo-island arc formed prior to the opening of the Shikoku basin (see Fig. 1 for the location). Ueda pointed out that almost all seamounts are magnetized in the normal direction, although the Nishi-shichito ridge in the Izu-Ogasawara arc and the Kyushu-Palau ridge were formed during the Oligocene to Miocene. The period contains frequent changes in magnetic polarity. He argued that such normal polarity bias suggests that IM contributes significantly to the magnetization of arc seamounts or that volcanic activities are more robust in the normal chron than in reverse chron. Ueda (2007) also pointed out that the Horeki seamount is normally magnetized and is not uniformly magnetized. The non-uniform magnetization probably indicates that NRM has some degree of contribution to the magnetization of the seamount.

Reversed magnetization is dominant in the eastern part of the northern ridges. The magnetization is consistent with the rock's age obtained from the ridge in this part (2.07 Ma; Figs. 3 and 11); therefore, the volcanism of these ridges is estimated to be active in Matuyama chron (2.58–0.78 Ma). The age of the young rock is obtained from the western part of the northern ridges (0.48 Ma, Fig. 3) where, in contrast, consistently normal magnetization is evaluated (Brunhes chron: 0.78 Ma–present).

The southern part of the seamount flanks, where small volcanic cones are well developed, is magnetized relatively normally with a very low magnitude. However, the flank is not different from other flanks in the density structure. Therefore, such a low magnitude of magnetization is probably caused by magnetization of the small cones. The small cones could have significant NRM because these cones are supposed to be monogenetic volcanoes and consist almost entirely of extrusive lavas. There are two alternate models that could explain the low magnetization. The first is that a number of volcanic cones erupted evenly during various ages, resulting in randomization of their remnant magnetization (Fig. 12(c)). The alternating structure of normal and reversed magnetization, which is approx. 1 km in size in the horizontal plane, does not affect the sea-surface magnetic anomaly, as suggested in the forward modeling shown in Fig. 8.

The second possibility is that many of the cones erupted in Matuyama chron (Fig. 12(d)). The reversed magnetization nearly cancels the normal magnetization of the main body. At present, we cannot distinguish between these models. The age of a rock sample obtained from one of the small cones shows a Gauss chron (Figs. 3 and 11). Additional age results from other small cones will be needed to resolve this question.

Otherwise, it cannot be ruled out that the origin may arise from non-uniform magnetization of the relatively deeper part. Rocks in this part have the same densities but do not have the same magnetization intensities, thereby reflecting difference in the magnetic field polarity, acquiring process of NRM, or degree of low/high-temperature oxidations of magnetic minerals.

There is no strong geological or seismological evidence to constrain the structure in the vertical extent. To advance the discussion, a near seafloor magnetic survey will reveal the more detailed structure and the nature of arc seamount's magnetization. Combined with the sea-surface survey, the magnetization in the shallower and deeper parts of seamount can be discussed. The near seafloor survey also improves the horizontal resolution of the structural analysis; consequently, the magnetization of each small volcanic cones in the southern part of seamount flanks can be examined. Therefore, the magnetization structure provides significant evidence for the acquisition of NRM, later volcanism, or degree of hydrothermal circulation of the arc seamount.

7. Conclusions

We conducted multi-beam bathymetry, gravity, and magnetic surveys of the Horeki back-arc seamount in the Izu-Ogasawara intra-oceanic arc, the western Pacific, to constrain the crustal structure and evolution. Our analysis of these data yielded the following results:

1. The flanks of the Horeki seamount show a higher density anomaly. The density of approx. 2800–2900 kg/m^3 corresponds to dense basaltic rocks.
2. A lower density anomaly is distributed in the top part of the Horeki seamount, parallel to the long axis. The resultant density is approx. 2500–2600 kg/m^3. The top part of the seamount is estimated to consist of porous basaltic rocks or differentiated rocks.

3. The prominent circular low Bouguer gravity anomaly appeared in the northern part of flat-topped summit. Rather light-density material filling the flat-topped summit is required.
4. The main body of the Horeki seamount is normally magnetized. The resultant low magnitude of magnetization is probably attenuated by integration of magnetization of the volcanic lavas that erupted in different magnetic chrons in history, resulting in natural remanent magnetization of opposite magnetic polarity. The totally normal magnetization indicates the volcanism constructing the main body may be more robust in the Gauss normal magnetic chron (3.58–2.58 Ma).
5. The deeper and inner part of the Horeki seamount may consist of intrusive rocks. The intrusive rocks having induced magnetization may contribute to the normal magnetization of the main body. The upper part of the seamount does not affect the bulk magnetization due to mixing of normal and reversed natural remanent magnetization carried by extrusive lavas and/or more differentiated rocks with low magnetization.
6. The reversed magnetization is consistent with the rock's age of 2.07 Ma obtained from the eastern part of the northern ridges; therefore the volcanism of these ridges is estimated to be active in the Matuyama chron (2.58–0.78 Ma). The western part of the northern ridges is normally magnetized, consistent with the sampled rock's age of 0.48 Ma (Brunhes chron: 0.78 Ma–present).
7. The southern part of the Horeki seamount flanks, where small volcanic cones are well-developed, has very weak normal magnetization. Such a low magnitude of magnetization is probably caused by magnetization of the small cones. A number of volcanic cones erupted evenly in various ages, resulting in randomization of their remnant magnetization. Otherwise, many of the cones erupted in Matuyama chron. Their reversed magnetization nearly cancels the normal magnetization of the main body.

Acknowledgments. We are grateful to the officers and crew of R/V *Kairei* for their outstanding professionalism and dedication that made the cruise successful. We thank the KR04-04 scientific party for collaboration and discussion. We are indebted to marine technicians from Nippon Marine Enterprises and Marine Works Japan for their invaluable help at sea. We thank A. Nishizawa for discussion regarding the OBS survey, N. Takahashi, K. Takizawa, and J.-O. Park for discussion regarding the MCS profile in KR02-05. We thank M. Hyodo, Y. Ueda, and an anonymous reviewer for their helpful comments in improving the manuscript. JTOPO30 published by Marine Information Research Center, Japan Hydrographic Association was used to fill the unsurveyed area. Observed geomagnetic data at the Hachijo Hydrographic Observatory operated by the Hydrographic and Oceanographic Department were used for correcting the diurnal variation. The GMT software (Wessel and Smith, 1995) was extensively used in this study. Part of this work is a contribution of the research program at the IFREE JAMSTEC.

References

Bhattacharyya, B. K., Magnetic anomalies due to prism-shaped bodies with arbitrary polarization, *Geophysics*, **29**, 517–531, 1964.

Blakely, R. J., *Potential Theory in Gravity & Magnetic Applications*, 441 pp., Cambridge University Press, New York, 1996.

Cande, S. C. and D. V. Kent, Revised calibration of the geomagnetic polarity time scale for the Late Cretaceous and Cenozoic, *J. Geophys. Res.*, **100**, 6093–6095, 1995.

Fujiwara, T., Gravity anomaly of the Izu-Bonin Island Arc, *Eos Trans. AGU*, **85**(28), *West. Pac. Geophys. Meet. Suppl.*, Abstract V33C-01, 2004.

Fujiwara, T., Y. Kido, Y. Tamura, and O. Ishizuka, Gravity and magnetic constraints on the crustal structure and evolution of the Horeki seamount in the Izu-Bonin arc, *JAMSTEC Rep. Res. Dev.*, **4**, 55–65, 2006.

Geological Survey of Japan, Gravity CD-ROM of Japan, 2000.

International Association of Geodesy (IAG), Geodetic Reference System 1967, Bureau Central de A. I. G. Spec. Pub. 3, 1967.

International Association of Geomagnetism and Aeronomy (IAGA), Division V, Working Group 8, The 9th generation International Geomagnetic Reference Field, *Earth Planets Space*, **55**, i–ii, 2003.

Ishizuka, O., K. Uto, M. Yuasa, and A. G. Hochstaedter, Volcanism in the earliest stage of back-arc rifting in the Izu-Bonin arc revealed by laser-heating $^{40}Ar/^{39}Ar$ dating, *J. Volcanol. Geotherm. Res.*, **120**, 71–85, 2002.

Ishizuka, O., R. N. Taylor, J. A. Milton, and R. W. Nesbitt, Fluid-mantle interaction in an intra-oceanic arc: constraints from high-precision Pb isotopes, *Earth Planet. Sci. Lett.*, **211**, 221–236, 2003a.

Ishizuka, O., K. Uto, and M. Yuasa, Volcanic history of the back-arc region of the Izu-Bonin (Ogasawara) Arc, in *Intra-Oceanic Subduction Systems: Tectonic and Magmatic Processes*, edited by R. D. Larter and P. H. Leat, Geol. Soc. Spec. Publ., **219**, 187–205, 2003b.

Ishizuka, O., R. N. Taylor, J. A. Milton, R. W. Nesbitt, M. Yuasa, and I. Sakamoto, Variation in the source mantle of the northern Izu arc with time and space—Constraints from high-precision Pb isotopes—, *J. Volcanol. Geotherm. Res.*, **156**, 266–290, 2006.

Ishizuka, O., R. N. Taylor, J. A. Milton, R. W. Nesbitt, M. Yuasa, and I. Sakamoto, Processes controlling along-arc isotopic variation of the southern Izu-Bonin arc, *Geochem. Geophys. Geosyst.*, Q06008, 10.1029/2006GC001475, 2007.

Kaiho, Y., N. Takahashi, T. Sato, G. Fujie, S. Kodaira, and Y. Kaneda, Wide-angle seismic profiling of oceanic island arc in the southern Izu-Ogasawara arc—KY0502 cruise—, *JAMSTEC Rep. Res. Dev.*, **3**, 43–52, 2006.

Kido, Y., Geophysical features of the north Izu-Ogasawara region, *Chikyu Monthly*, **52**, 104–112, 2005 (in Japanese).

Kodaira, S., T. Sato, N. Takahashi, A. Ito, Y. Tamura, Y. Tatsumi, and Y. Kaneda, Seismological evidence for variable growth of crust along the Izu intraoceanic arc, *J. Geophys. Res.*, **112**, doi: 10.1029/2006JB004593, 2007a.

Kodaira, S., T. Sato, N. Takahashi, S. Miura, Y. Tamura, Y. Tatsumi, and Y. Kaneda, New seismological constraints on growth of continental crust in the Izu-Bonin intra-oceanic arc, *Geology*, **35**, 1031–1034, 2007b.

Koyama, M., S. M. Cisowski, and P. Pezard, Paleomagnetic evidence for northward drift and clockwise rotation of the Izu-Bonin forearc since the early Oligocene, In Taylor, B., Fujioka, K. *et al.*, *Proc. ODP, Sci. Results*, **126**, College Station, TX (Ocean Drilling Program), 353–370, 1992.

Kuo, B. Y. and D. W. Forsyth, Gravity anomalies of the ridge-transform system in the South Atlantic between 31° and 34.5°S: Upwelling centers and variations in crustal thickness, *Mar. Geophys. Res.*, **10**, 205–232, 1988.

Lin, J., G. M. Purdy, H. Schouten, J.-C. Sempéré, and C. Zervas, Evidence from gravity data for focused magmatic accretion along the Mid-Atlantic Ridge, *Nature*, **344**, 627–632, 1990.

Ludwig, W. J., J. E. Nafe, and C. L. Drake, Seismic refraction, in *The Sea*, 4, edited by A. E. Maxwell, 53–84, Wiley-Interscience, New York, 1970.

Miura, S., T. Sato, T. No, N. Takahashi, S. Kodaira, and Y. Kaneda, Wide-angle seismic experiment crossing the Sofu-gan tectonic line in the Izu-Ogasawara arc—KY0502 cruise—, *JAMSTEC Rep. Res. Dev.*, **3**, 19–29, 2006.

Murakami, F. and T. Ishihara, Submarine caldera discovered in the northern Izu-Bonin arc, *Chikyu Monthly*, **7**, 638–646, 1985 (in Japanese).

Nishizawa, A., K. Kaneda, A. Nakanishi, N. Takahashi, and S. Kodaira, Crustal structure of the ocean-island arc transition at the mid Izu-Ogasawara (Bonin) arc margin, *Earth Planets Space*, **58**, e33–e36, 2006.

Park, J.-O., T. Tsuru, Y. Kido, M. K. Thu, S. Kodaira, and Y. Kaneda, Multichannel seismic reflection image across the Izu-Bonin island arc

system—preliminary results—, *Fall meeting, Seismo. Soc. Japan*, P071, 222, 2002.

Press, W. H., S. A. Teukolsky, W. T. Vetterling, and B. P. Flannery, *Numerical Recipes: The Art of Scientific Computing*, Cambridge University Press, New York, 963 pp., 1992.

Prince, R. A. and D. W. Forsyth, Horizontal extent of anomalously thin crust near the Vema Fracture Zone from the three-dimensional analysis of gravity anomalies, *J. Geophys. Res.*, **93**, 8,051–8,063, 1988.

Sandwell, D. T. and W. H. F. Smith, Marine gravity anomaly from Geosat and ERS 1 satellite altimetry, *J. Geophys. Res.*, **102**, 10,039–10,054, 1997.

Shipboard Scientific Party, Site 1256, In Wilson, D. S., Teagle, D. A. H., Acton, G. D., *et al.*, *Proc. ODP, Init. Repts.*, **206**: College Station, TX (Ocean Drilling Program), 1-396, 10.2973/odp.proc.ir.206.103.2003, 2003.

Shukuno, H., Y. Tamura, K. Tani, Q. Chang, T. Suzuki, and R. S. Fiske, Origin of silicic magmas and the compositional gap at Sumisu submarine caldera, Izu-Bonin arc, Japan, *J. Volcanol. Geotherm. Res.*, **156**, 187–216, 2006.

Takahashi, N., S. Kodaira, T. Sato, A. Ito, T. No, and Y. Kaneda, Wide-angle seismic profiling of arc-arc collision zone in the northern Izu-Ogasawara arc—KY0408 cruise—, *JAMSTEC Rep. Res. Dev.*, **1**, 23–36, 2005.

Tamura, Y., K. Tani, O. Ishizuka, Q. Chang, H. Shukuno, and R. S. Fiske, Are arc basalts dry, wet, or both? Evidence from the Sumisu caldera volcano, Izu-Bonin arc, Japan, *J. Petrol.*, **46**, 1769–1803, 2005.

Tamura, Y., O. Ishizuka, H. Shukuno, H. Kawabata, K. Tani, T. Fujiwara, Y. Kido, and R. S. Fiske, Horeki backarc volcano of the Izu-Bonin arc, Japan Geoscience Union Meeting, J161-035, 2006.

Tamura, Y., K. Tani, Q. Chang, H. Shukuno, H. Kawabata, O. Ishizuka, and R. S. Fiske, Wet and dry basalt magma evolution at Torishima volcano, Izu-Bonin arc, Japan: the possible role of phengite in the downgoing slab, *J. Petrol.*, **48**, 1999–2031, 2007.

Tani, K., R. S. Fiske, Y. Tamura, Y. Kido, J. Naka, H. Shukuno, and R. Takeuchi, Sumisu volcano, Izu-Bonin arc, Japan: site of a silicic caldera-forming eruption from a small open-ocean island, *Bull. Volcanol.*, **70**, 547–562, 2008.

Tatsumi, Y., The subduction factory: how it operates in the evolving Earth, *GSA Today*, **15**, 4–10, 2005.

Tsuru, T., J.-O. Park, T. No, K. Takizawa, and Y. Kaneda, Cruise report of 2004 seismic reflection surveys in Izu-Ogasawara Arc, *JAMSTEC Rep. Res. Dev.*, **2**, 1–12, 2005.

Ueda, Y., Magnetic and gravity field analyses of Izu-Ogasawara (Bonin) Arc and their tectonic implications, *J. Geomag. Geoelectr.*, **48**, 421–445, 1996.

Ueda, Y., Magnetizations of the seamounts in the Izu-Ogasawara arc with special reference to the origin of their normal polarity biases, *Earth Planets Space*, **59**, 897–909, 2007.

Wessel, P. and W. H. F. Smith, New version of Generic Mapping Tools released, *EOS Trans. AGU*, **76**, 329, 1995.

Yamazaki, T. and M. Yuasa, Possible Miocene rifting of the Izu-Ogasawara (Bonin) arc deduced from magnetic anomalies, *Island Arc*, **7**, 374–382, 1998.

T. Fujiwara (e-mail: toshi@jamstec.go.jp), Y. Kido, Y. Tamura, and O. Ishizuka